

## Fourier-Expansion Solution of Atom Distributions in a Crystal Using X-Ray Standing Waves

L. Cheng,<sup>1</sup> P. Fenter,<sup>1</sup> M. J. Bedzyk,<sup>1,2</sup> and N. C. Sturchio<sup>1,3</sup>

<sup>1</sup>Argonne National Laboratory, Argonne, Illinois 60439, USA

<sup>2</sup>Northwestern University, Evanston, Illinois 60208, USA

<sup>3</sup>University of Illinois at Chicago, Chicago, Illinois 60607, USA

(Received 3 December 2002; published 27 June 2003)

Term-by-term Fourier-expansion series, each made up of components having element-specific phases and amplitudes acquired with x-ray standing wave measurements on successive orders of Bragg reflections, are used to reconstruct impurity atom distributions in muscovite mica with respect to the (001) lattice without *a priori* assumptions on their structures.

DOI: 10.1103/PhysRevLett.90.255503

PACS numbers: 61.10.-i, 68.49.Uv

Model independence in crystallographic structural determination is a key criterion for achieving reliable, unique solutions. Conventional applications of x-ray and neutron diffraction suffer from phase ambiguity because these methods measure only scattered intensities rather than (complex) amplitudes. This “phase problem” prevents direct Fourier inversion of reciprocal-space data to direct-space structures. To recover phases indirectly from intensity distributions, considerably complex statistics-based retrieval procedures, known as “direct methods,” are required [1]. Alternatively, only a few other techniques can achieve phase sensitivity at the atomic scale; examples are methods based on multiple-beam diffraction [2,3], multiple scattering [4], and electron and x-ray holographies [5–9].

Atomic characteristic emission excited by an x-ray standing wave (XSW) field during an  $H$  ( $= hkl$ ) Bragg diffraction is explicitly sensitive to the phase (and the amplitude) of the  $H$ th Fourier component  $\rho_H(\mathbf{r})$  of an atom crystallographic distribution  $\rho(\mathbf{r}) = \sum \rho_H(\mathbf{r})$  with respect to the  $H$  lattice [10–12]. Therefore, for atoms with characteristic emissions, XSW can be used as a tool for collecting a complete set of phases and amplitudes; these data can then be Fourier inverted to give the direct-space, element-specific atom crystallographic distributions without *a priori* assumptions on their structures. This procedure provides a new way for uniquely profiling arbitrary bulk-impurity and surface-adsorbate distributions if the substrate crystal structure is known.

The mathematical criterion for Fourier representation of an arbitrary (unknown) distribution function requires a formal (term-by-term) expansion series. For the purpose of attaining crystallographic resolution, this series must also be sufficiently extended. To acquire phases and amplitudes for such a series demands XSW measurements be made on successive orders of Bragg reflections along a given  $H$ . These measurements would necessarily span a large range in reciprocal space, a requirement practically prevented by instrumental limitations in the past [13]. As a result, in previous applications of XSW, measurements have been made on selected—rather than a complete,

multiple-order set of—Bragg reflections; interpretations of these data require references to models, which restrict applications to only simple structures.

Using high-brilliance synchrotron x rays and high-phase-resolution monochromators (Advanced Photon Source, beam line 12ID-D) [14], we have made XSW measurements on the first eight orders of allowed  $(00l)$  Bragg reflections of a muscovite mica crystal, i.e.,  $l = 2, 4, \dots, 16$ . These measurements explicitly provide the phases and amplitudes for up to the eighth term in a term-by-term Fourier expansion of atom distributions within the fundamental 002 unit cell. Here, we show that the Fourier-inverted structures of lattice cations quantitatively reproduce their known structures, and we use this method to determine the model-independent distributions of impurity cations with respect to the known muscovite (001) lattice. We also discuss how this method can in principle be extended to systems without known substrate structures.

Muscovite ( $2M_1$ ) has unit-cell parameters  $a = 5.19 \text{ \AA}$ ,  $b = 9.01 \text{ \AA}$ ,  $c = 20.05 \text{ \AA}$ , and  $\beta = 95.78^\circ$ . Its end-member formula is  $\text{K}_2\text{Al}_4(\text{Si}_3\text{Al})_2\text{O}_{20}(\text{OH})_4$  [15]. In the fundamental 002 unit cell, the three lattice cations are distributed differently—K is located at an interlayer site, Si is equally distributed at two tetrahedral sites, and Al is unequally distributed at an octahedral site and the tetrahedral sites. This range of distributions offers an assessment on the effectiveness of the method in adequately resolving fairly complex structures with finite numbers of orders of XSW measurements.

X-ray beams were monochromated at 7.44 keV with a Si(111) monochromator and further collimated with a Si postmonochromator under detune (at  $\sim 50\%$ ). Postmonochromator Si crystal reflections were chosen to best match the sample reflections to minimize dispersion. The Si(111) reflection was used for the muscovite (002), (004), and (006) reflections; Si(022) for the muscovite (008) and (0010) reflections; and Si(004) for the muscovite (0012), (0014), and (0016) reflections. As the sample was rotated through each  $(00l)$  reflection, the reflectivity and the atomic x-ray fluorescence

emissions were recorded with an ionization counter and a solid-state detector, respectively. The fluorescence emissions were acquired at low takeoff angles (typically  $\sim 6^\circ$ ) from the sample surface.

The reflectivity  $R_H(\theta)$  and the phase of the XSW field  $\phi_H(\theta)$  across an  $H$  Bragg reflection are determined by a fit to the experimental reflectivity using the dynamical diffraction theory and the known muscovite structure factors. The normalized fluorescence yield of an atomic emission is [11–14]

$$Y_H = 1 + R_H + 2\sqrt{R_H}F_H \cos(\phi_H - 2\pi P_H)Z_H, \quad (1)$$

where the effective thickness  $Z_H(\theta)$  accounts for the extinction effect [12,14]; the coherent fraction  $F_H$  and coherent position  $P_H$ —both having normalized values ranging from 0 to 1—are the amplitude and phase (in the prefactor) of the  $H$ th component of the Fourier-expansion representation of an atom distribution as projected into the crystallographic unit cell [11–14]. In terms of  $F_H$  and  $P_H$ , an element-specific atom density distribution  $\rho(\mathbf{r})$  in a unit cell can be written as

$$\rho(\mathbf{r}) = \rho_0 \sum_H F_H \exp[-2\pi i(\mathbf{H} \cdot \mathbf{r} - P_H)], \quad (2)$$

where  $\rho_0$  is the fractional atom density of the unit cell,  $\mathbf{r} = x\mathbf{a} + y\mathbf{b} + z\mathbf{c}$ , and  $\mathbf{H} = h\mathbf{a}^* + k\mathbf{b}^* + l\mathbf{c}^*$ .

Since the muscovite structure is centrosymmetric along the  $(00l)$  plane normal, Eq. (2) can be rewritten

for a one-dimensional distribution in this direction as

$$\rho(z) = \rho_0 \left[ 1 + 2 \sum_l F_{00l} \cos 2\pi(lz - P_{00l}) \right], \quad (3)$$

where the summation is over all positive allowed  $l$ . With the XSW data acquired for  $l = 2, 4, \dots, 16$ , the series is carried out to the eighth term. The value of  $\rho_0$  for each element was determined by normalizing the element's fractional atom density to that of oxygen, which has the known absolute density of 24 oxygens per muscovite formula unit. The fractional densities of all elements in the sample were measured using quantitative wavelength-dispersive x-ray fluorescence spectroscopy.

The reflectivity and normalized fluorescence yields of the lattice atoms (K, Si, Al) and cation impurities (Mn, Fe, Ti, Ba) measured across each of the  $(00l)$  Bragg reflections, and their best  $\chi^2$  fits according to Eq. (1), are shown in Fig. 1. From the best fits, the amplitudes  $F_{00l}$  and phases  $P_{00l}$  of each element's distribution are obtained. The  $P_{00l}$  values are with respect to the chosen unit-cell origin at the octahedral site. The XSW-measured  $F_{00l}$  and  $P_{00l}$  values are plotted in Fig. 2. For the lattice atoms, the XSW-measured  $F_{00l}$  are compared with a set of calculated  $F_{00l}$  based on the end-member structure and the known temperature factors [15]. Good agreement is generally observed in these comparisons. Occasional discrepancies, mostly in having lower measured  $F_{00l}$  values, can be attributed to contributions of fluorescence signals

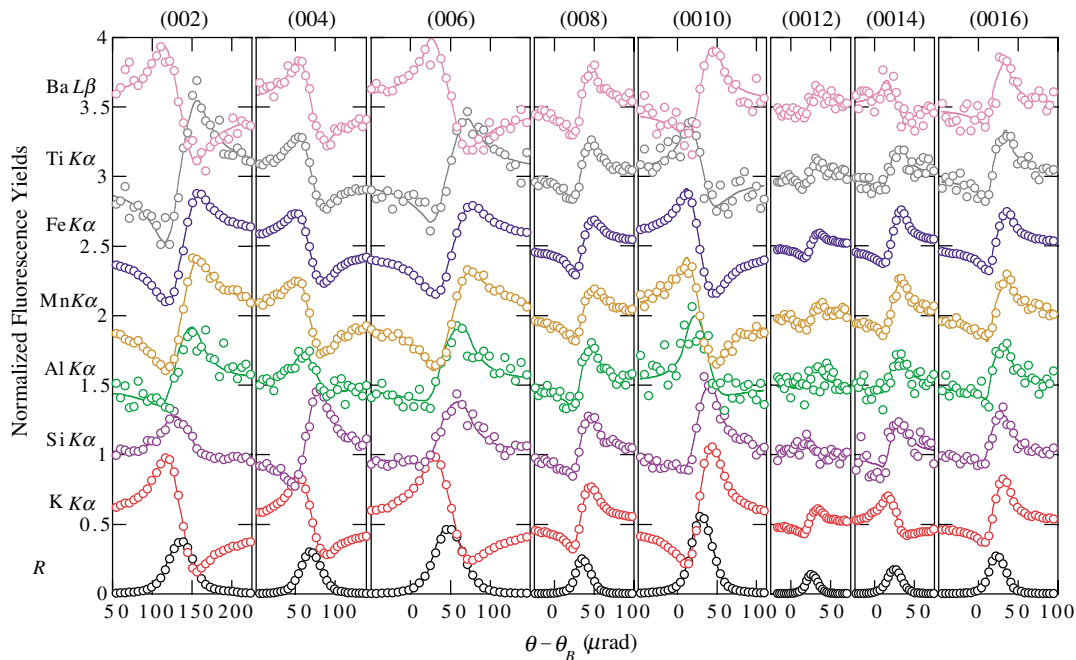


FIG. 1 (color). Experimental data and best-fit curves for reflectivity ( $R$ ) and normalized fluorescence yields for lattice atoms (K, Si, Al) and impurities (Mn, Fe, Ti, Ba) in muscovite around the allowed  $(00l)$  Bragg reflections up to  $l = 16$ . The angle  $\theta$  is the incident angle of x rays, and  $\theta_B$  is the  $(00l)$  geometric Bragg angle. For clarity, the fluorescence yields are shifted on the vertical axis, in order, by  $-0.5, 0, 0.5, 1, 1.5, 2,$  and  $2.5$ , respectively.

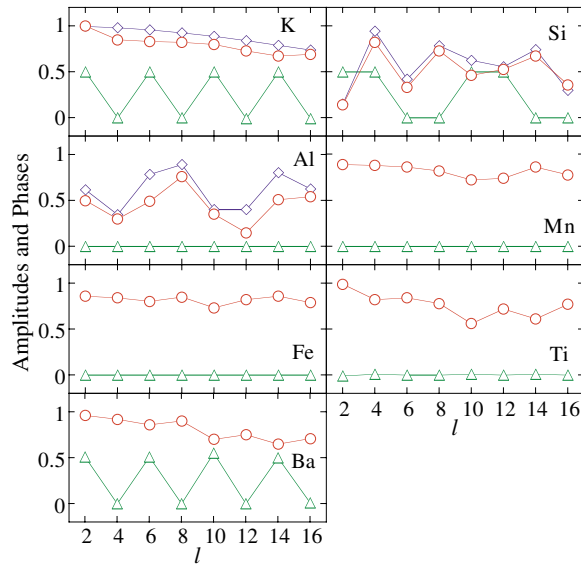


FIG. 2 (color). XSW-measured amplitudes  $F_{00l}$  (circles) and phases  $P_{00l}$  (triangles) of the  $00l$  Fourier components of the distributions of lattice atoms (K, Si, Al) and impurities (Mn, Fe, Ti, Ba), and the calculated amplitudes  $F_{00l}$  (diamonds) for lattice atoms.

not from the coherently diffracting region of the sample. For  $P_{00l}$ , on the other hand, the XSW-measured values are consistently in good agreement with the calculated values (which, by symmetry, are 0 or 0.5), typically within the statistical uncertainty of  $\sim \pm 0.02$ .

The reciprocal-space XSW data in Fig. 2 are directly Fourier inverted according to Eq. (3) to give the direct-space atom density distributions. Figure 3 shows the density distributions of the seven elements; the peaks indicate the locations of atom sites. The observed FWHM of the peaks is  $\sim 0.8 \text{ \AA}$ ; this value is close to the expected resolution of  $\frac{1}{2}d_{0016} = 0.62 \text{ \AA}$ , limited by the termination  $l$  value of the Fourier series. Finite termination also causes artificial background oscillations in the density profiles, but these oscillations can be suppressed by using a suitable window function, e.g., the Hanning window [16]. The one-dimensional density profiles obtained here can be combined with additional profiles similarly reconstructed from XSW measurements in noncollinear directions to generate full three-dimensional atom density profiles [17].

To evaluate the accuracy of the density profiles, we compare in Fig. 3 the lattice atom density distributions inverted from XSW-measured  $F_{00l}$  and  $P_{00l}$  and from calculated  $F_{00l}$  and  $P_{00l}$ . The positions of corresponding peak maxima are generally in agreement within  $\sim 0.02 \text{ \AA}$ , consistent with the high phase sensitivity of the XSW method. Specifically, with respect to the 001 unit cell, K is located at  $z = \pm \frac{1}{4}$  (the interlayer sites), Si is located in equal occupation at  $z = \pm 0.137$  and  $\pm(\frac{1}{2} - 0.137)$  (the tetrahedral sites), and Al is located at  $z = 0$

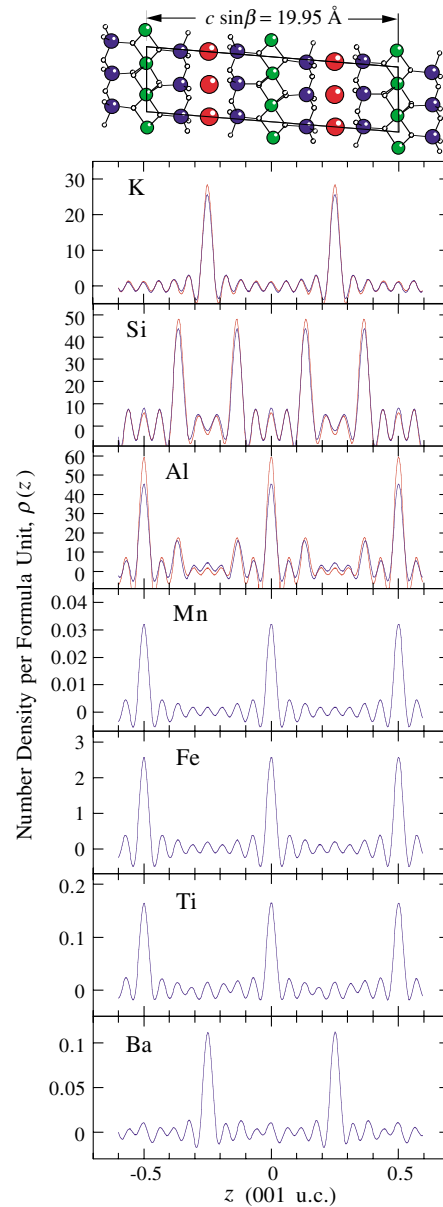
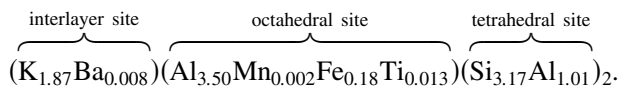


FIG. 3 (color). Density distributions of lattice atoms (K, Si, Al) and impurities (Mn, Fe, Ti, Ba) in the muscovite 001 unit cell according to Fourier-expansion solutions using XSW-measured amplitudes and phases (blue lines) and, for lattice atoms, amplitudes and phases based on crystallographic data (red lines). A unit-cell model is drawn to scale with the density distributions. The atoms at the interlayer sites, the tetrahedral sites, and the octahedral sites are shown in red, blue, and green, respectively.

and  $\frac{1}{2}$  (the octahedral sites) as well as the tetrahedral sites. The experimentally derived occupations of the lattice atoms are also in general agreement with the calculated occupations. The only significant discrepancy, in Al occupation at the octahedral sites, is likely due to intrinsic differences between the sample and the end-member structure in Al occupation at these sites, as well as to the larger errors in measured  $F_{00l}$  (discussed above).

The model-independent distributions for the impurity atoms in Fig. 3 reveal that Mn, Fe, and Ti are located at the octahedral sites, and Ba is located at the interlayer sites. From the determined atom distributions, the (detected) cation portion of the muscovite formula can be reconstructed as



The stoichiometry represented in this partial formula is consistent with that of a typical natural muscovite sample [18].

In this study, we have made use of the known muscovite structure factors in determining the reflectivity  $R_H(\theta)$  and the XSW phase  $\phi_H(\theta)$ , which are required for Eq. (1). Given this process, the derived impurity distributions are model-independent structures with respect to the known muscovite lattice. However, if the bulk crystal structure were not known, atom crystallographic distributions could in principle still be determined through an iterative process without reference to *a priori* known bulk structure factors. This more arduous, completely model-independent element-specific crystallographic determination for impurities as well as lattice atoms is possible because the reflectivity data (shown in the bottom of Fig. 1) are acquired with a high-resolution diffractometer with absolute angle and reflectivity scales. The angular positions of the Bragg peaks give the lattice constants, and the Darwin widths extracted from the reflectivity curves determine the moduli of the structure factors. Ignoring x-ray absorption effects,  $R_H(\theta)$  and  $\phi_H(\theta)$  can be calculated in the first iteration without using structure factors.

Fourier inversion to direct-space atom distributions using XSW data are in principle analogous to Fourier inversion using x-ray diffraction data with retrieved phases. Among the strengths of the XSW approach are its elemental specificity and superior sensitivity to dilute atom concentrations, reaching the order of 500 ppm [19]. The XSW-based method is also fully applicable to the determination of adsorbate species where the substrate crystal structure is known. The limitations of the XSW-based method are that its applications require high-quality single crystals whose diffraction conforms with the dynamical theory (although generalization of this method may be extended to thin-film XSW and total external reflection XSW [14]). This method is also restricted to elements whose characteristic x-ray fluorescence or electron emissions are detectable. In addition, for bulk fluorescence emissions, proper selection of incident x-ray energy may be required to minimize potential secondary emissions [12].

Overall, the XSW-based Fourier-expansion solution offers an alternative to diffraction-based inversion methods for achieving unique solutions for arbitrary atom distributions in crystals. This method is expected to be particularly useful for solving complex bulk-impurity and surface-adsorbate structures.

This work was supported by the Geosciences Research Program of the Office of Basic Energy Sciences, the U.S. Department of Energy, through Contract No. W-31-109-ENG-38 to Argonne National Laboratory, and was conducted at the Advanced Photon Source and at the X-ray Diffraction Facility at Northwestern University (supported by NSF Contracts No. DMR-0076097 and No. CHE-9810378). We thank J. Carsello and Z. Zhang for assistance.

- 
- [1] See, e.g., C. Giacovazzo, *Direct Methods in Crystallography* (Academic Press, London, 1980).
  - [2] Q. Shen and K. D. Finkelstein, *Phys. Rev. Lett.* **65**, 3337 (1990).
  - [3] Q. Shen, *Phys. Rev. Lett.* **80**, 3268 (1998).
  - [4] D. K. Saldin, A. Seubert, and K. Heinz, *Phys. Rev. Lett.* **88**, 115507 (2002).
  - [5] S. Omori *et al.*, *Phys. Rev. Lett.* **88**, 055504 (2002).
  - [6] H. Wu *et al.*, *Phys. Rev. Lett.* **89**, 216101 (2002).
  - [7] M. Tegze and G. Faigel, *Nature (London)* **380**, 49 (1996).
  - [8] T. Gog *et al.*, *Phys. Rev. Lett.* **76**, 3132 (1996).
  - [9] M. Kopecky, A. Lausi, E. Busetto, J. Kub, and A. Savoia, *Phys. Rev. Lett.* **88**, 185503 (2002).
  - [10] B. W. Batterman, *Phys. Rev. Lett.* **22**, 703 (1969).
  - [11] N. Hertel, G. Materlik, and J. Zegenhagen, *Z. Phys. B* **58**, 199 (1985).
  - [12] M. J. Bedzyk and G. Materlik, *Phys. Rev. B* **32**, 6456 (1985).
  - [13] J. Zegenhagen, *Surf. Sci. Rep.* **18**, 199 (1993).
  - [14] M. J. Bedzyk and L. Cheng, in *Reviews in Mineralogy and Geochemistry*, edited by P. Fenter *et al.* (Mineralogical Society of America, Washington, 2002), Vol. 49, p. 221.
  - [15] M. F. Brigatti, P. Frigieri, and L. Poppi, *Am. Mineral.* **83**, 775 (1998).
  - [16] W. H. Press and S. A. Teukolsky, *Numerical Recipes* (Cambridge University Press, New York, 1996), 2nd ed.
  - [17] J. A. Golovchenko, J. R. Patel, D. R. Kaplan, P. L. Cowan, and M. J. Bedzyk, *Phys. Rev. Lett.* **49**, 560 (1982).
  - [18] M. F. Brigatti and S. Guggenheim, in *Reviews in Mineralogy and Geochemistry*, edited by A. Mottana *et al.* (Mineralogical Society of America, Washington, 2002), Vol. 46, p. 1.
  - [19] L. Cheng, N. C. Sturchio, and M. J. Bedzyk, *Phys. Rev. B* **63**, 144104 (2001).